

Alternating Flux Barrier Design of Vernier Ferrite Magnet Machine Having High Torque Density

Wenbo Liu

Department of Electrical and Computer Engineering
University of Wisconsin
Madison WI, USA
Wliu86@wisc.edu

Thomas A. Lipo

Department of Electrical and Computer Engineering
University of Wisconsin
Madison WI, USA
lipo@engr.wisc.edu

Abstract—This paper proposes a new topology for a single air gap spoke type vernier permanent magnet (SVPM) machine, that uses only ferrite permanent magnets (PMs), where alternating flux barriers are placed at the bottom of pair-wise magnets on the rotor. Overall, the alternating flux barrier topology reduces the manufacturing complexity, mechanical structural challenges and thermal issues, which are predominant problems for existing high torque density spoke type vernier machine solutions having a dual stator topology. In this paper, design innovations, obtained through analytical analysis and detailed discussion, are verified using finite element analysis (FEA). These results show that the improved SVPM design not only improves the torque density compared to that of the conventional SVPM by 57% but also effectively reduce the torque ripple down to 7.6%, the torque production even surpasses that of a benchmark rare earth interior permanent magnet (IPM) machine under same size and stator current density. The comparison draws the conclusion that the new ferrite single air gap SVPM topology shows considerable promise in low and medium speed applications both as a motor or generator.

Keywords—vernier machine; spoke type; ferrite magnet; alternating flux barrier; low speed; high torque density

NOMENCLATURE

θ_s	Spatial angle of the stator MMF.
θ_r	Spatial angle of the rotor PM MMF.
θ_{rm}	Mechanical rotor rotation angle.
k_h	h^{th} harmonic winding factor.
N_t	Total number of turns.
I_{pk}	Stator peak current.
C_p	Number of parallel circuits.
P_s, P_r	Number of stator poles, and number of rotor poles.
S_s	Number of stator slots.
γ	Current phase shift angle.
p_0, p_h	dc and h^{th} harmonic component of air gap permeance
F_{pmgh}	h^{th} harmonic component of the rotor PM MMF.
B_{gap}	Air gap flux density.
H_{gap}	Air gap magnetic field intensity.
V_{gap}	Air gap volume.

d_{is}	Inner stator radius.
l_i	Stack length.

I. INTRODUCTION

The vernier machine (VM) was first introduced as a synchronous reluctance machine variant less than 60 years ago [1], and a permanent magnet version of this type of machine has appeared only a little more than 20 years ago [2]. The term vernier is used to describe the feature that, the rotor of this machine rotates relatively slowly, only at a definite fraction of the angular speed of the stator rotating field. Meanwhile, the motor torque steps up as the rotor speed steps down. This so-called electric gearing effect makes the VM an attractive alternative for direct-drive applications, where vibration, acoustic noise and reliability of conventional gear systems are the major concerns [3]. Torque production is effectively improved in surface mount type vernier permanent magnet machine (VPM) compared to the reluctance type design [2], [4], [5], [6]. Furthermore, the dual excitation structure and double rotor structure increase the machine airgap surface area [4], [5], [6], which improve the torque density by nearly 50% compared to a single rotor and single excitation design. However, the surface mount type VPM retains low power factor as the downside because the magnets added to the rotor creates additional harmonic flux leakage in the air gap [4], [5].

To cope with the low power factor issue of VPMs, a dual stator spoke type vernier permanent magnet motor (DSSVPM) has been proposed. The adoption of spoke type magnets not only reduces the airgap distance compared to surface mount type VPMs, but also takes advantage of a flux focusing effect, thus the motor torque density is also enhanced [7], [8], [9]. Due to the large amount of magnet usage in this machine, efforts on reducing the active material cost have also been pursued by replacing rare earth PMs used in DSSVPMs by ferrite PMs along with a detailed demagnetization analysis in [8].

On the other hand, the downsides of dual excitation structure and double rotor structure are obvious and inevitable. The introduction of one more layer of rotor or one more layer of stator significantly increases the machine manufacturing complexity, and poses a challenge to mechanical structural integrity as well. The thermal issue becomes another concern since the inner stator is enclosed by rotating parts which limits the cooling options for windings situated in that area. As a

result of the drawbacks stated above, VPMs presently have few applications in the industry. Therefore, a practical design more suitable for massive production with competitive performance is in great need to bridge the gaps between VPM research and industry adoption.

This paper introduces a novel single air gap spoke type Vernier permanent magnet machine (SVPM) with alternating flux barrier design. Ferrite magnets are used as a replacement for rare earth magnets to reduce the active material cost of the VPM. The proposed SVPM is simulated in 2D FEA. Key results are benchmarked against a conventional ferrite SVPM and an existing low speed commercial available IPM using rare earth magnets.

II. OPERATING PRINCIPLE

The VPM operates similar to an electric gear in which rotor torque is produced at a different frequency from the rotating frequency. Since the rotor flux is spatially modulated by a pulsating toothed stator permeance, the operating principle is analogous to frequency modulation in communication theory. To illustrate the spatial modulation of the rotor magnetic field and magnetic coupling in torque production, a generic spoke type VPM is shown in Fig. 1(a), as the counter-clock wise direction indicates the positive angle notation.

Like a normal sequenced three phase stator, a rotating magnetomotive force (MMF) will be built up at the temporal frequency of armature excitation. The corresponding analytical expression of this MMF is described in (1), where the \pm sign suggests that this wave can rotate either counter-clock wise or clock wise. The air gap permeance (p_g) due to the pulsating stator tooth can be described as in (2). On the other side of air gap, the rotor consists of a ring shape iron core with spoke array magnets inserted radially with opposing magnetization direction for adjacent magnets, thus the rotor PM MMF can be expressed as in (3). Consequently, the rotor flux density in the air gap after modulation can be obtained,

which is calculated as product of the rotor PM MMF and the stator air gap permeance, then divided by airgap surface area. The flux density produced by the fundamental component of (2) and (3) is listed in (4), where $c_1 = F_{pmg1} p_1 / 2$, $c_0 = F_{pmg1} p_0 / 2$.

$$F_{sg} = \sum_{h=1,5,7,11\dots} \left(\frac{3}{2} \cdot \frac{4}{\pi} \right) \frac{k_r N_r I_{pk}}{h C_p P_s} \cos \left(h \frac{P_s}{2} \theta_s \pm (\omega_e t - \gamma) \right) \quad (1)$$

$$p_g = p_0 + p_h \sum_{h=1,3,5\dots} \cos(h S_s \theta_s) \quad (2)$$

$$F_{pmg} = F_{pmgh} \sum_{h=1,3,5\dots} \cos \left(h \left(\frac{P_r}{2} \right) \theta_r \right) \quad (3)$$

$$B_{rg} = \left\{ c_1 \cos \left(\frac{P_r}{2} \theta_r - S_s \theta_s \right) + c_0 \cos \left(\frac{P_r}{2} \theta_r \right) + c_1 \cos \left(\frac{P_r}{2} \theta_r + S_s \theta_s \right) \right\} / (\pi d_{is} l_i) \quad (4)$$

Demonstration waveforms along the air gap circumference representing (1)–(4) are shown in Fig. 1(b), with an example structure having 4 stator poles, 20 rotor magnets. A unit magnitude is assumed for each waveform, where the major harmonic coupling components for torque production are highlighted in green, black, and magenta corresponding to 20-poles, 4-poles and 44-poles, respectively. In VPMs, certain slots and pole number combination must be satisfied in order to enable the vernier effect, the combination can be determined by inspecting the rotor torque equation, which can be expressed as the rate of change of the field energy stored in the air gap as:

$$T = \frac{\partial}{\partial \theta_{rm}} \left[\int_{V_{gap}} B_{gap} H_{gap} dV_{gap} \right] \approx \frac{d_{is} l_i}{2} \int_0^{2\pi} \left(\frac{\partial}{\partial \theta_{rm}} B_{rg} \right) F_{sg} d\theta_s \quad (5)$$

If one substitutes $\theta_r = \theta_s - \theta_{rm}$ to B_{rg} in (5), the integration becomes:

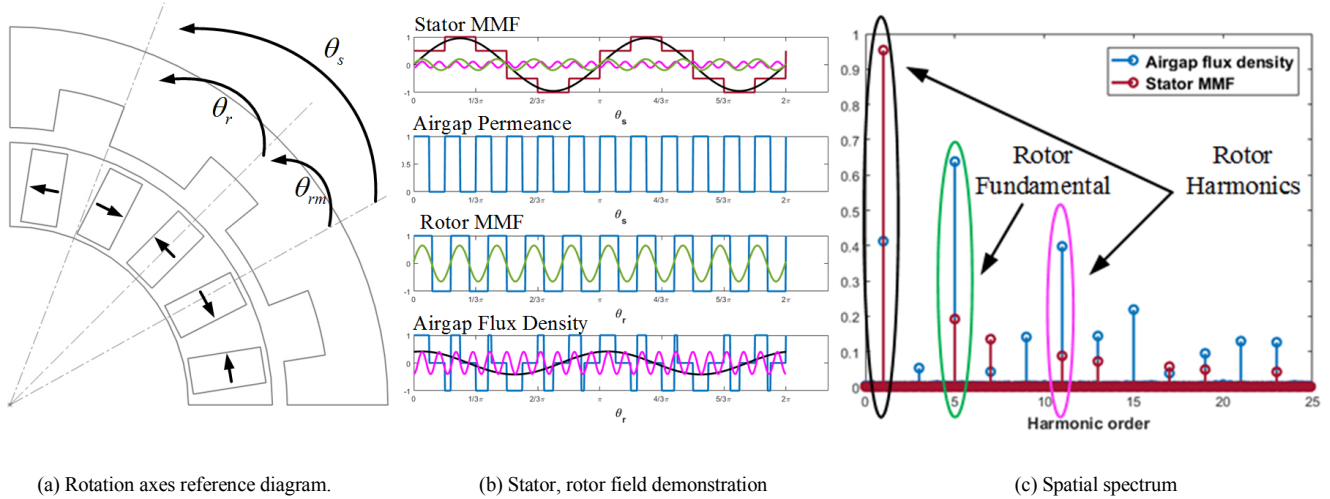


Fig. 1. Demonstration of a spoke type VPM and corresponding field distribution

$$T = \frac{3}{2\pi^2} \frac{N_t I_{pk} P_r}{C_p P_s} \int_0^{2\pi} \left\{ \sum_{h=1,5,7,11,\dots} \frac{k_h}{h} \cos\left(h \frac{P_s}{2} \theta_s \pm (\omega_s t - \gamma)\right) \times \right. \\ \left. \left[c_1 \sin\left(\left(\frac{P_r}{2} - S_s\right) \theta_s - \frac{P_r}{2} \theta_{rm}\right) + c_0 \sin\left(\frac{P_r}{2} (\theta_s - \theta_{rm})\right) + \right. \right. \\ \left. \left. c_1 \sin\left(\left(\frac{P_r}{2} + S_s\right) \theta_s - \frac{P_r}{2} \theta_{rm}\right) \right] \right\} d\theta_s \quad (6)$$

It should be noted that up to three components can be spatially coupled between the stator MMF (cosine term in (6)) and the air gap flux density (sine terms in (6)) to produce torque, and to maximize the torque production, it is desired to couple as many lower order stator MMFs as possible. Thus, the fundamental component of stator MMF should share the same spatial frequency with the first term of B_{rg} as:

$$\pm \frac{P_s}{2} = \frac{P_r}{2} - S_s \quad (7)$$

where $\pm P_s/2$ both represent the same fundamental stator spatial MMF. The other two terms in B_{rg} can then be uniquely determined by coupling with the following two stator MMF harmonics for a given number of stator poles (P_s) as:

$$\begin{aligned} -\frac{P_s}{2} = \frac{P_r}{2} - S_s, h=1 & \quad +\frac{P_s}{2} = \frac{P_r}{2} - S_s, h=1 \\ 5\frac{P_s}{2} = \frac{P_r}{2}, h=5 & \quad 7\frac{P_s}{2} = \frac{P_r}{2}, h=7 \\ 11\frac{P_s}{2} = \frac{P_r}{2} + S_s, h=11 & \quad 13\frac{P_s}{2} = \frac{P_r}{2} + S_s, h=13 \end{aligned} \quad (8)$$

If one further considers an ideal fully pitched concentrated winding, which has been found to be a preferred choice to levitate power factor for the VPM [10], the stator slot number can be calculated as: $S_s = 3P_s$. Fig. 1(c) shows the harmonic spectrum analysis both of the stator MMF and the air gap flux density, as the '-' sign is selected in (7). The spectrum analysis suggests that the example VPM has three major field coupling components, where one of them is the fundamental field similar to a normal 20-pole synchronous PM machine; the other two are harmonic fields which are extra components that also contribute to torque production. It should now be clear that, due to the modulation effects on the rotor field, two extra rotor harmonic fields can be coupled with stator MMF to generate average torque.

Since there are two designs of slot and pole number combination as shown in (7), a primitive quantitative comparison can be carried out to determine which one provides more torque. If one assumes the motor is tuned to operate at the maximum torque per ampere point, the torque of two designs in (6) can be written as:

$$T_+ = \frac{3}{4\pi^2} \frac{N_t I_{pk} P_r}{C_p P_s} F_{pmg1} \left(p_1 \frac{k_1}{1} + p_0 \frac{k_7}{7} + p_1 \frac{k_{13}}{13} \right) \quad (9)$$

$$T_- = \frac{3}{4\pi^2} \frac{N_t I_{pk} P_r}{C_p P_s} F_{pmg1} \left(p_1 \frac{k_1}{1} + p_0 \frac{k_5}{5} + p_1 \frac{k_{11}}{11} \right) \quad (10)$$

where T_{\pm} corresponds to $P_r = 2S_s \pm P_s$, respectively.

If one ignores skew and slot effects, the winding factor would then be essentially unity and the ratio of the torque production of the two designs can be simplified as:

$$T_+ / T_- = 7 \left(p_1 \frac{14}{13} + p_0 \frac{1}{7} \right) / \left(5 \left(p_1 \frac{12}{11} + p_0 \frac{1}{5} \right) \right) \quad (11)$$

Assuming $p_0 = p_1$, then $T_+ / T_- \geq 1.32$ is obtained, which indicates that ideally $P_r = 2S_s + P_s$ design would produce 32% more torque compared to $P_r = 2S_s - P_s$ design by having a larger rotor pole number. Regardless of choice of rotor pole number between the two cases, the term P_r / P_s in (9) and (10) reveals the gear effect in the VPM. Thus far, the derivation is completely based on a generic VPM. The useful insights observed above will be now be used for the analysis of the new design in the following section.

III. ALTERNATING FLUX BARRIER DESIGN

Although the VPMs are inherently equipped with a gear down effect with a gear ratio of P_r / P_s , which is ideal for low speed direct drive application, the existing topologies of this kind of machine pose challenges for industry adoption as: either it would be complex and difficult to build for double stator topologies [7], [8], or it would require oversized inverter to drive the poor power factor machine for single stator topologies [11]. This section introduces an alternating flux barrier design on the rotor of a SVPM, which can simplify manufacturing process while keeping a reasonable power factor. A proposed and a conventional SVPM design using ferrite magnets are first compared, then the two designs are benchmarked against a commercial available IPM using rare earth magnets for industrial cooling fan application.

Following the derivations of previous section, A 4 stator pole, 20 rotor pole SVPM of the conventional topology and the proposed topology are shown in Fig. 2. For conventional topology, as a zoomed-in rotor view in Fig. 2(a) suggests, the rotor radial space is mostly occupied by the ferrite magnets with thin iron bridge on the top and bottom to hold the magnets in place. For the proposed design in Fig. 2(d), an alternating flux barrier structure is placed on the bottom of pair-wise spoke type magnets. The barriers need to be of low permeability material, which are connected by a thin iron bridge, the iron bridge can help limit axial leakage flux at the rotor ends and eliminate unbalanced force [12]. The corresponding no load flux line distributions are shown in Fig. 2(b), and (e), where the flux from rotor magnets that links to the coil set A can be extracted by simple inspection: two major rotor magnet flux paths specified in red and orange, that links to coil A in the conventional SVPM design can be observed in Fig. 2(b), with colored arrows indicating the corresponding flux direction. By adopting the proposed design, there are three major rotor magnet flux paths, linking

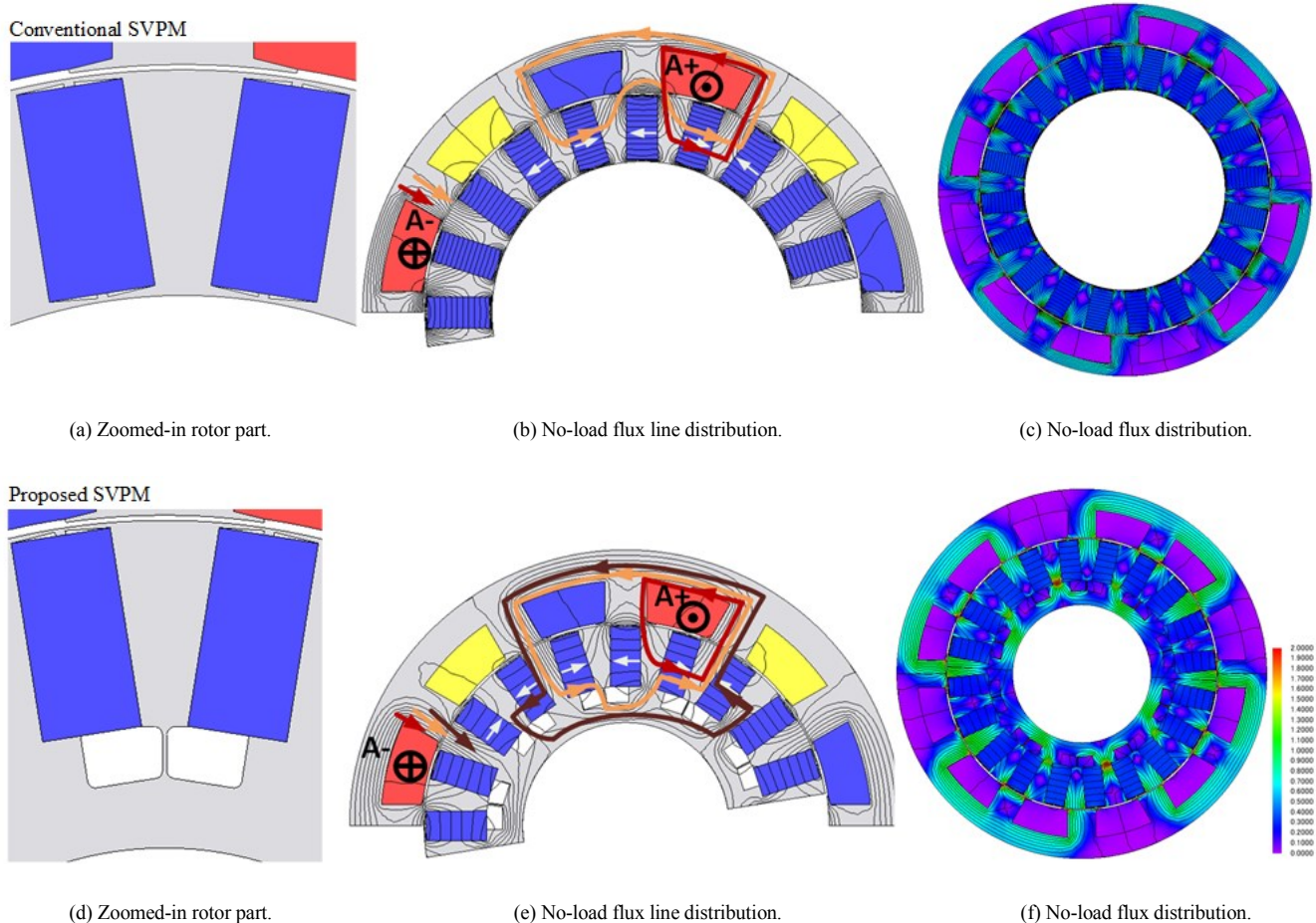


Fig. 2. Conventional design and alternating flux barrier design with no-load study

four magnets to coil A. The extra iron space created in between pair-wise adjacent magnets is also a part of the flux path colored in brown, and associated with the remaining portion of the iron path on rotor, it helps include two additional magnets linking coil A. It also should be noted that the alternating use of rotor flux barriers allows the use of an enlarged rotor back iron without producing a magnetic short circuit of the rotor magnets. This result is verified by the no load flux distribution plots in Fig.2(c), and (f), where the flux leakage in the air gap and in the leakage iron path is greatly reduced. As a result, more flux links the stator coil as shown in Fig. 2(f) compared to that of the conventional SVPM shown in Fig. 2(c).

In addition, the new design provides a flux path not only for the magnet flux but also for the stator MMF at rated load. Thus, the stator MMF does not need to traverse across the spoke type magnets which act effectively as large air gaps. The major stator MMF drop that previously existed across these large rotor air gaps is significantly reduced, which means the inductances seen by the stator is inversely increased. The power factor improvement of this machine might be limited as a result. The value $P_r = 2S_s - P_s$ has been chosen here due to the challenge of fitting thick ferrite magnets to the limited rotor space. This would not be a

problem should the machine have a larger diameter and the results, shown to be favorable in the next section, could even be greater.

TABLE I. DESIGN KEY DIMENSIONS

	Proposed SVPM	Conventional SVPM
Stator OD/ID [mm]	355.6/261.7	355.6/278
Rotor OD/ID [mm]	259.7/133	276/191
D_{cs} [mm]	19.8	11.3
D_{cr} [mm]	13.5	-
τ_s [°]	30	30
τ_{pr} [°]	18	18
t_s [mm]	26.5	26.6
d_{pm}/w_{pm} [mm]	20.8/38.9	20/39.5
d_{bg1}/d_{bg2} [mm]	0.5/0.8	0.8/0.8
d_b/w_b [mm]	14.6/10.4	-

The proposed SVPM using ferrite magnets was designed according to the discussion in previous section for industrial cooling fan application. The geometry of the proposed

topology was carefully characterized as shown in Fig. 3. The detailed design and optimization process will be provided in a subsequent paper. Here only the optimization results for machine geometry in Table I are shown for both a proposed topology and a conventional topology, where maximizing the average torque and minimizing the ripple torque are set as the primary optimization target.

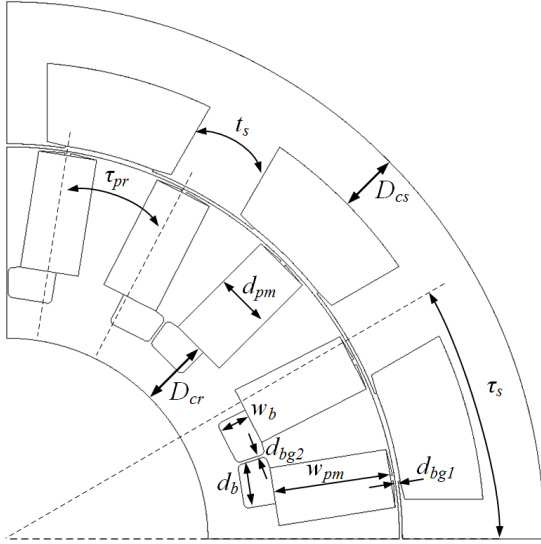


Fig. 3. Parametrization of the proposed machine geometry

To make a fair comparison between conventional SVPM, proposed SVPM and an existing, commercially available benchmark IPM by a major motor manufacturer. The machine outer stator diameter and stack length are kept the same, as well as the stator current density. A comparison of key performance features are tabulated in Table II.

A more detailed performance comparison is shown in Fig. 4. Fig. 4(a) shows a no load back-emf comparison which indicates that the back-emf of the proposed SVPM has a more sinusoidal shape and larger magnitude than that of the

conventional design. Fig. 4(b) shows a transient torque comparison at rated load condition where the proposed design not only achieves a better average torque but also manages to reduce the torque ripple from 18.3% down to 7.6%. A torque versus current plot at the MTPA operating point analysis is shown in Fig. 4(c). The plot indicates that the proposed SVPM generally improves the torque production over the entire current/load range, and increases by 57% compared to that of a conventional SVPM at rated load, which equivalently improves torque density by the same amount. The torque capability of the proposed SVPM design even surpasses that of an existing rare-earth IPM machine as shown in Table II. The tradeoff for this result is that the magnet weight is increased while the power factor is lowered due to the use of ferrite magnets. However, only minimum modifications were made to the alternating flux barrier SVPM to achieve the degree of performance improvement listed above.

IV. CONCLUSION

An alternating flux barrier SVPM has been proposed in this paper using ferrite PMs. The FEA results suggest that the proposed SVPM not only improves the torque density by 57% of the conventional SVPM, but also reduces the torque ripple by nearly a factor of 3. The torque production also surpasses that of a benchmark rare earth magnets assisted IPM under the same stator current density condition, with the tradeoff as: the magnet weight is increased while the power factor is lowered due to the use of ferrite magnets. A significant amount of material cost reduction is also obtained by adoption of ferrite material. Overall, the simple structure and good torque capability make the proposed single air gap alternating flux barrier SVPM an attractive and practical alternative for low speed applications, like industrial cooling fans, wind turbines, and marine propulsion.

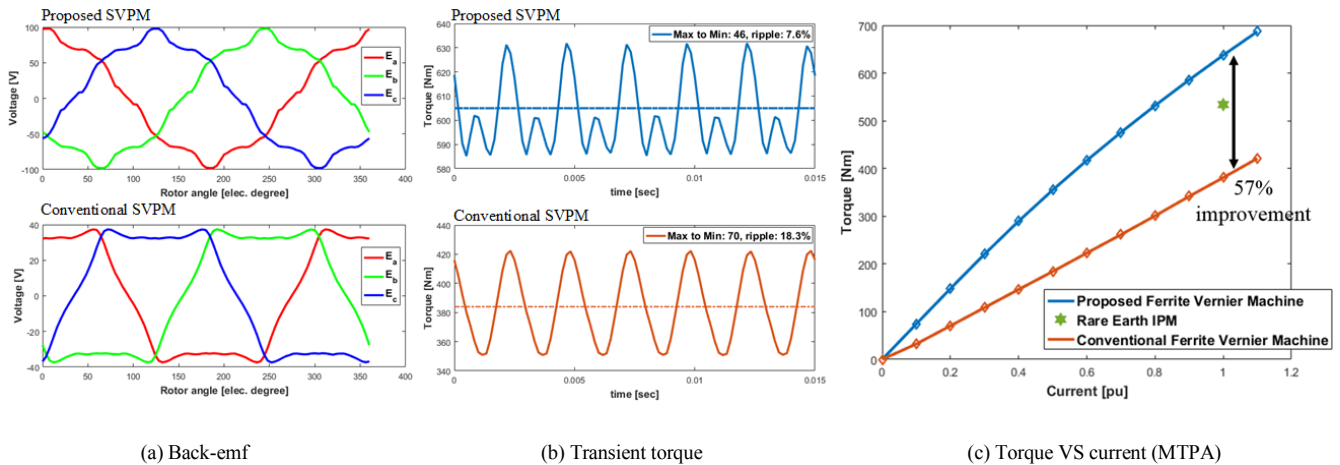


Fig. 4. Detailed performance comparison

TABLE II. KEY PARAMETERS AND PERFORMANCE COMPARISON

	Benchmark motor	Proposed SVPM	Conventional SVPM
Machine type	IPM	VPM	VPM
Magnet type/Br [T]	NdFeB/1.2	Ferrite/0.42	Ferrite/0.42
Stator/rotor pole number	4/4	4/20	4/20
SPP	4	1	1
J_s [A/mm ²]	4.6	4.6	4.6
Excitation frequency, [Hz]	13.33	66.67	66.67
PM mass/% of total weight [kg]	11.3/3.6%	25.2/8%	24.8/7.9%
Cu vol. (incl. end wind.) [L]	3.1	3.5	3.5
Torque [Nm]	534	605	384
Torque density (over total vol.) [Nm/L]	17.3	19.4	12.2
Power factor [lagging]	0.8	0.62	0.61

ACKNOWLEDGMENT

The authors express their gratitude to the companies of the Wisconsin Electric Machines and Power Electronics Consortium (WEMPEC) for assistance and support during this research

REFERENCES

- [1] C. H. Lee, "Vernier motor and its design," *IEEE Trans. Power Appar. Syst.*, vol. 82, no. 66, pp. 343–349, 1963.
- [2] A. Ishizaki, T. Tanaka, K. Takahashi, and S. Nishikata, "Theory and Optimum Design of PM Vernier Motor." Electrical Machines and Drives Seventh International Conf., Durham, UK, 1995.
- [3] R. Qu, D. Li, and J. Wang, "Relationship between magnetic gears and vernier machines," in *Electrical Machines and Systems (ICEMS), 2011 International Conference on*, 2011, pp. 1–6.
- [4] A. Toba and T. A. Lipo, "Novel dual-excitation permanent magnet vernier machine," in *Industry Applications Conference, 1999. Thirty-Fourth IAS Annual Meeting. Conference Record of the 1999 IEEE*, 1999, vol. 4, pp. 2539–2544.
- [5] A. Toba and T. A. Lipo, "Generic torque-maximizing design methodology of surface permanent-magnet vernier machine," *IEEE Trans. Ind. Appl.*, vol. 36, no. 6, pp. 1539–1546, 2000.
- [6] S. Niu, S. L. Ho, W. N. Fu, and L. L. Wang, "Quantitative Comparison of Novel Vernier Permanent Magnet Machines," *IEEE Trans. Magn.*, vol. 46, no. 6, pp. 2032–2035, Jun. 2010.
- [7] D. Li, R. Qu, and T. A. Lipo, "High-Power-Factor Vernier Permanent-Magnet Machines," *IEEE Trans. Ind. Appl.*, vol. 50, no. 6, pp. 3664–3674, Nov. 2014.
- [8] Z. S. Du and T. A. Lipo, "High torque density ferrite permanent magnet vernier motor analysis and design with demagnetization consideration," in *Energy Conversion Congress and Exposition (ECCE), 2015 IEEE*, 2015, pp. 6082–6089.
- [9] B. Kim and T. A. Lipo, "Analysis of a PM Vernier Motor With Spoke Structure," *IEEE Trans. Ind. Appl.*, vol. 52, no. 1, pp. 217–225, Jan. 2016.
- [10] B. Kim and T. A. Lipo, "Operation and Design Principles of a PM Vernier Motor," *IEEE Trans. Ind. Appl.*, vol. 50, no. 6, pp. 3656–3663, Nov. 2014.
- [11] J. Li, K. T. Chau, J. Z. Jiang, C. Liu, and W. Li, "A New Efficient Permanent-Magnet Vernier Machine for Wind Power Generation," *IEEE Trans. Magn.*, vol. 46, no. 6, pp. 1475–1478, Jun. 2010.
- [12] X. Ge, Z. Q. Zhu, J. Li, and J. Chen, "A Spoke-Type IPM Machine With Novel Alternate Airspace Barriers and Reduction of Unipolar Leakage Flux by Step-Staggered Rotor," *IEEE Trans. Ind. Appl.*, vol. 52, no. 6, pp. 4789–4797, Nov. 2016.